JOURNAL OF GEOPHYSICAL RESEARCH, VOL. 96, SUPPLEMENT, PAGES 3249–3262, FEBRUARY 28, 1991

Equatorial Kelvin and Rossby Waves Evidenced in the Pacific Ocean Through Geosat Sea Level and Surface Current Anomalies

THIERRY DELCROIX, JOËL PICAUT, AND GÉRARD ELDIN

Groupe SURTROPAC, Institut Français de Recherche Scientifique pour le Développement en Coopération (ORSTOM), Nouméa, New Caledonia

Abstract. Equatorial Kelvin and Rossby waves are comprehensively demonstrated over most of the equatorial Pacific basin, through their signatures in sea level and zonal surface geostrophic current anomalies. This was made possible with altimeter data pertaining to the first year of the Geosat (Geodetic Satellite) 17-day exact repeat orbit (November 8, 1986, to November 8, 1987). To this end, along-track corrected Geosat sea level anomalies (SLAs), relative to the time period of interest, were first smoothed using nonlinear and linear filters. The original 17-day time step was then reduced by combining all ascending and descending tracks within 10° longitudinal bands. Finally, SLAs were gridded onto a regular grid, and low-pass filters were applied in latitude and time in order to smooth out remaining high-frequency noise. Anomalies of zonal surface geostrophic current were calculated using the first and second derivatives of the SLA meridional gradient, off and on the equator, respectively. Sea level and surface current anomalies are validated in the western equatorial Pacific with in situ data gathered during seven hydrographic cruises at 165°E, and through expendable bathythermograph and mooring measurements. Following their chronological appearance along the 165°E meridian, the major low-frequency SLAs and zonal surface current anomalies are described and explained in terms of the equatorial wave theory. An equatorial downwelling Kelvin wave, known to be the main oceanic signal of the 1986-1987 El Niño, is generated in December 1986, concomitant with a strong westerly wind anomaly occurring west of the dateline. The associated propagating equatorial SLAs correspond to an elevation of 15 cm. Independent estimates of this Kelvin wave phase speed are obtained through time-lag correlation matrix analysis (2.82 ± 0.96 m s^{-1}) and the least squares fit of the SLA meridional structures to theoretical Kelvin wave shape (2.26 ± 1.02 m s^{-1}). Both estimates indicate that the Kelvin wave has the characteristic of a first baroclinic mode. An equatorial upwelling Kelvin wave is then detectable in June 1987. It is characterized by a 10-cm sea level drop, propagating only from the western to the central equatorial Pacific. A first meridional mode (m=1) equatorial upwelling Rossby wave crossing the entire Pacific basin from March 1987 (eastern part) to September 1987 (western part) shows up in SLAs and zonal surface current anomalies. Such a Rossby wave corresponds to propagating sea level drops which are extreme (-12 cm) at about 4°N and 4°S latitudes. The consequences on zonal surface geostrophic current are very important since, in the case of the upwelling, it dramatically decreases the three major surface currents (the North and South Equatorial Countercurrents, and South Equatorial Current) by an amplitude similar to their mean annual velocity values. The least squares fit of the Rossby wave SLA meridional structures to its theoretical m=1 form cogently suggests the dominance of the first baroclinic mode (c=2.59 ± 0.65 m s^{-1}). This dominance is corroborated by an estimate of the Rossby wave phase speed (1.02 ± 0.37 m s^{-1}), which roughly corresponds to the theoretical phase speed ($c/2m+1$) of the m=1 equatorial Rossby wave. It is suggested that the equatorial upwelling Rossby wave is mostly due to a reflection of an equatorial upwelling Kelvin wave generated in January 1987 near the dateline. Whether or not the overall propagating features are part of the 1986-1987 El Niño or belong to the "normal" seasonal cycle cannot be decided in the absence of longer altimeter sea level time series.

1. INTRODUCTION

The theory of equatorial waves was presented more than 20 years ago in the seminal works of *Matsuno* [1966], *Moore* [1968], and *Lighthill* [1969]. Recent developments have tremendously increased our knowledge and understanding of the low-latitude ocean circulation, and clearly bring out the role of equatorial waves in the adjustment of the ocean mass and velocity structures to external forcing (cf. summaries by *Moore and Philander* [1977]; *Philander* [1978]; *Cane and Sarachik* [1983]; *Knox and Anderson* [1985]; *Eriksen and Katz* [1987]).

From an observational point of view, the related equatorial Kelvin and Rossby waves were only documented fairly recently. Low-frequency equatorial Kelvin waves were first suspected in the early 1980s through the meridional shape of their sea level signature [*Ripa and Hayes*, 1981], and then detected as an eastward propagating pulse in zonal near-surface current [*Knox and Halpern*, 1982]. Subsequently, quite a lot of observations (cf. *Eriksen and Katz* [1987] for a review) were interpreted in terms of equatorial Kelvin waves. Unlike evidence of Kelvin waves, observational evidence of equatorial Rossby waves is still scarce, and limited either to their zonal propagation between a few locations [*Lukas et al.*, 1984] or to their meridional structures at one specific longitude [*Lukas and Firing*, 1985]. To the authors's knowledge, a comprehensive analysis of an observed equatorial Rossby wave is still lacking, in contrast with the now well-documented off-equatorial Rossby wave [e.g., *Emery and Magaard*, 1976; *White*, 1977; *Meyers*, 1979; *Kessler*, 1990]. Definite observational evidence of equatorial Rossby waves would thus be an important milestone in equatorial ocean dynamics, considering the key role they play in the adjustment of tropical ocean models [e.g., *McCreary*, 1976, 1985; *Busalacchi and O'Brien*, 1981; *Battisti*, 1989].

For technical and dynamical reasons, sea level (or surface dynamic height) is the most commonly used parameter that enables detection of the signature of an equatorial Kelvin wave, both in models and observations. *Miller et al.* [1988] nicely demonstrate an equatorial Kelvin wave propagation over most of the Pacific, taking advantage of the unprecedented spatial/temporal sea level coverage provided by Geosat (Geodetic Satellite). Satellite measuring provides the only way

Paper number 90JC01758.
0148-0227/91/90JC-01758$05.00

of obtaining basin-wide sea level observations over a long time period. Hence it plays a major role in quasi-real-time monitoring of the oceans (cf. *Climate Diagnostics Bulletin*, published by the Climate Analysis Center, National Meteorological Center, National Weather Service, NOAA, Washington, D.C.) and the past and anticipated results meet most of the goals expressed in climate-related programs such as the Tropical Ocean and Global Atmosphere (TOGA) and World Ocean Circulation Experiment (WOCE) programs [cf. *Stewart and Lefebvre*, 1987].

Cheney and Miller [1988] demonstrate the usefulness of Geosat in describing the sea level variability during the 18-month classified geodetic mission and approximately 7-month Exact Repeat Mission (ERM). *Tai et al.* [1989] verify the validity of altimetric sea level versus dynamic height field derived from expendable bathythermograph (XBT) and island sea level data. *Miller et al.* [1988] detect equatorial Kelvin wave propagation during the 1986-1987 El Niño / Southern Oscillation (ENSO), and *Miller and Cheney* [1990] present results showing large-scale sea level fluctuations and changes in upper layer volume in the tropical Pacific during the 4-year period from April 1985 to February 1989. To date, there has been only one attempt to derive geostrophic zonal surface current at the equator from Geosat measurements. *Picaut et al.* [1990], through a comparison with in situ near-surface zonal current, show that meaningful geostrophic surface current estimates can be deduced from Geosat sea level, right at the equator. Our present investigation complements and tries to go further than these Geosat tropical ocean-related studies.

The purpose of our paper is, from the Geosat ERM data for the 1986-1987 ENSO period, to investigate cross-Pacific propagations of equatorial Kelvin waves and, for the first time, of an equatorial Rossby wave. These propagations will be documented and analyzed both in terms of Geosat sea level anomalies (GSLA) and surface geostrophic zonal current anomalies (GZCA). We will investigate whether these equatorial waves have the characteristics of a first baroclinic mode via several independent phase speed estimates. Namely, we will use time-lag correlation analysis to determine the zonal propagation, and will adjust the equatorial meridional trapping scale of these waves to the theoretical shapes through a least squares fit. Tentative explanations for the origin of the equatorial Kelvin and Rossby waves are also proposed. We will show that wind stress anomaly forcing is consistent with Kelvin wave triggering, and that a first meridional mode Rossby wave observed all the way to the western Pacific may be the reflection of a Kelvin wave at the eastern Pacific coast.

The paper is organized as follows. In section 2 the processing of altimeter data is discussed, and an evaluation of Geosat sea levels in the western Pacific is presented. In section 3 the propagations of equatorial Kelvin and Rossby waves are analyzed according to their sequential appearance in the western equatorial Pacific. The related GZCA are examined further in section 4. Discussion and conclusions are presented in section 5.

2. DATA, DATA PROCESSING, AND EVALUATION

2.1. *Geosat Data*

Detailed information about the Geosat mission, as well as engineering and scientific papers, can be found in a review released by the Johns Hopkins Applied Physics Laboratory (*JHAPL*) [1987].

After 18 months of primary geodetic mission, Geosat was moved to a 72° orbit inclination for the 17-day ERM, which became fully operational on November 8, 1986. The ERM collinear ground tracks have an equatorial separation of 164 km (82 km with the combination of ascending and descending tracks), and the original 0.1-s sampling altimetric measurements averaged every 1-s result in a 6.8-km along-track resolution.

The data used in the present study correspond to the first 22 repeated cycles (November 8, 1986, to November 18, 1987). They were processed and kindly provided to us by Chet Koblinsky of the NASA Goddard Space Flight Center (NASA GFSC). The following briefly presents the corresponding processing. The along-track data were at first interpolated using a tenth-order Hermite interpolation algorithm. In a way similar to that of *Cheney et al.* [1987] the altimetric sea level data were corrected from tides [*Schwiderski*, 1980], sea state bias, wet troposheric refraction, and sea level pressure (the last two corrections based on the Navy Fleet Numerical Oceanographic Center model output). The satellite orbit was computed by the Navy Astronautics Group, using Doppler tracking from three stations. Following the technique recommended by *Cheney et al.* [1983], radial orbit error was removed from the mean collinear track detrended over 2500-km segments through the least squares fit quadratic function. In order to eliminate the mean geoid, the final sea level data set corresponds to collinear deviations from the means calculated over at least 20 out of the 22 original cycles. Data gaps, evident on Figure 1, are either due to less than 20 complete cycles or to data rejections resulting from standard deviation criteria over the original 0.1-s data [*Cheney et al.*, 1987]. Owing to the elimination of the mean, the mean sea surface topography is removed, and one must keep in mind that all the results of the present paper are relative to the average for the November 8, 1986, to November 18, 1987, period. Therefore we will only examine sea level anomaly (SLA) or current anomaly in the following sections.

2.2. *Data Processing*

Sea level gridding. Although the processed GSLA we obtained from NASA GFSC were already corrected for all environmental disturbances, additional filtering in space and time is required to remove remaining instrumental and/or oceanic noises. Figure 2 exemplifies a 30°S-30°N along-track GSLA, and clearly evidences the need to suppress nonphysical spikes, the largest occurring in the vicinity of the Intertropical Convergence Zone (ITCZ). Thus the first step of our own GSLA processing is to apply a nonlinear median filter on the along-track data, following *Picaut et al.*'s [1990] technique. These authors tested different filter lengths by comparing equatorial zonal surface geostrophic currents derived from GSLA and directly measured currents from equatorial moorings. Such comparisons constitute the most stringent test, since, on the equator, the geostrophic currents involving the meridional GSLA gradient are very sensitive to small-scale GSLA noises. Picaut et al. concluded that the best comparison is obtained when using a 400-km filter length, athough a 300 to 500-km filter length did not alter their result. This choice is consistent with the 400 to 600-km along-track decorrelation scale we found for GSLA data, as well as with the 300-km meridional decorrelation scale for thermal structure obtained in the tropical Pacific ocean [*White et al.*, 1985]. In order to keep maximum information on meridional (72° inclination) GSLA structure, we used a 300-km filter length. Figure 2 shows the effects of the 300-km nonlinear filter and indicates some residual irregularities, which were then smoothed with a

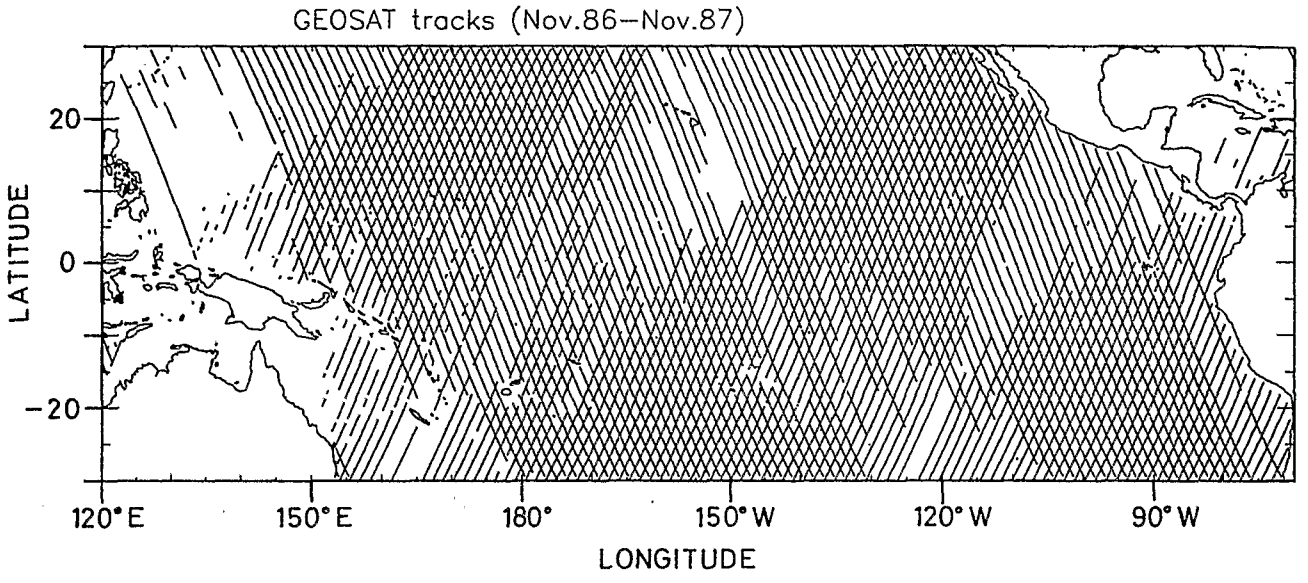

Fig. 1. Ground tracks of the Geosat 17-day repeat orbit over the tropical Pacific ocean.

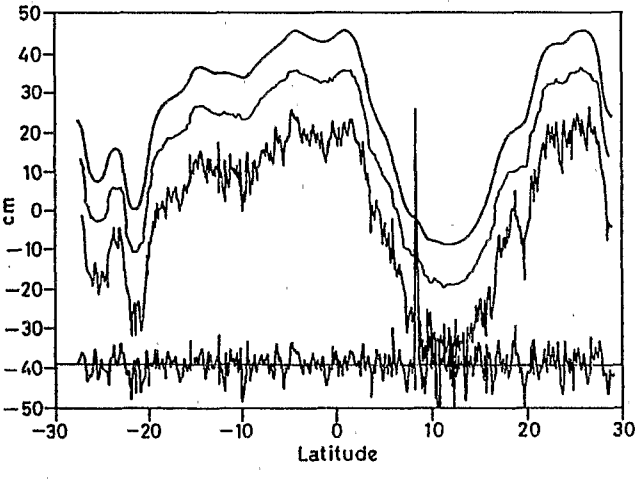

Fig. 2. Centered at zero are the corrected sea level anomalies for an individual Geosat pass. Shifted 10 cm above is the same along-track series after the application of a nonlinear median filter. The top curve is the processed along-track series after the application of a linear Hanning filter. The small-scale variability removed by the two-step filtering is depicted at the bottom (40-cm offset).

300-km linear Hanning filter [*Bendat and Piersol*, 1971]. The final result of the along-track filtering is shown on Figure 2 (top curve). Note that prior to along-track filtering, spurious jumps (not shown on Figure 2) resulting from interpolation between the two data points surrounding a gap were avoided through interpolation between the means computed on the two half filter lengths situated on each side of the gap.

The second step of our data processing is to grid the huge amount of GSLA data onto a regular space/time grid covering the whole tropical Pacific ocean (20°N-20°S; 150°E-80°W), for the November 8, 1986, to November 20, 1987, period. One goal of the present paper is to study equatorial Kelvin wave propagation. The original 17-day time step is obviously too coarse to quantitatively analyze such a fast propagation. However, the time step can be reduced by combining all ascending and descending tracks over zonal bands. This yields a 1.5-day resolution at the equator for a 9° zonal band, but is variable at higher latitudes (up to 5 days poleward of 15°). *Picaut et al.* [1990] use modeled sea level data sampled along the 17-day repeat orbit of the Geosat ERM to conclude that a 9°-10° longitude binning process does not seriously degrade the low-frequency estimation of the geostrophic flow field at the equator. A similar conclusion must apply for the sea level. The GSLA data were thus grouped in 10° zonal bands centered from 155°E to 85°W, and then gridded onto 0.5°-latitude and 5-day bins using the Laplacian interpolation scheme. (The region west of 150°E is not investigated owing to the poor coverage and quality of the GSLA data set). As a final processing, 31-day and 3°-latitude Hanning filters were applied to suppress remaining small-scale variability resulting from the time/space combination technique. It is worth mentioning that smoothing on the independent 10° zonal bands was not added in order to clearly resolve zonal propagation of equatorial waves.

Geostrophic current calculation. Low-frequency large-scale motions are in quasi-geostrophic balance. For the zonal component and with the standard notations, the mathematical expression for this balance is

$$f u = -\rho^{-1} p_y \qquad (1a)$$

Given the sea surface height η relative to the geoid, the corresponding surface geostrophic zonal current becomes

$$f u = -g \eta_y \qquad (1b)$$

Off the equator, zonal surface currents are calculated from our GSLA data, gridded every 0.5° of latitude, with a first-order centered finite difference scheme. On the equator, (1*a*) and (1*b*) are indeterminate. In order to calculate u on the equator, *Jerlov* [1953] first suggested using the second derivative of the meridional pressure field on an equatorial β-plane ($f=\beta y$), namely:

$$\beta u = -\rho^{-1} p_{yy} \qquad (2a)$$

or

$$\beta u = -g \eta_{yy} \qquad (2b)$$

This relation is applied with a finite second-derivative scheme on our GSLA data, sampled north, south, and at the equator. This second-derivative technique, applied to the same GSLA data, is adequate for estimating low-frequency surface equatorial zonal current with reasonable accuracy [*Picaut et al.*, 1990] (see section 4). Off the equator, there is general agreement that the first derivative of the meridional pressure field gives a reasonable low-frequency zonal current estimate. However, presence of a meridional pressure gradient in the equatorial wave guide (e.g., induced by a meridional wind stress) adds a frictional term to the geostrophic equation (equation (1)), destroys the corresponding geostrophic balance [*Joyce*, 1988], and induces a discontinuity between the surface zonal currents deduced from the first (equation (1)) and second (equation (2)) derivative. *Tournier* [1989] and *Picaut and Tournier* [this issue] discuss this question and suggest adding an equatorially trapped correction factor $C(y)$ to the meridional pressure field, so that

$$C(y) = (-p_y)_{y=0}\, y \exp(-y^2/L^2) \qquad (3)$$

which ensures continuity between the currents deduced from the first- and the second- derivative calculations. This technique does not alter the zonal current right on the equator. It just smoothes out the near-equatorial current irregularities induced by an equatorial meridional pressure gradient. A trapping scale L of 2° latitude is chosen for the present study, following *Picaut and Tournier* [this issue].

2.3. *Evaluation*

Sea level anomalies. Before using GSLA data to study sea level and derived surface geostrophic current variability, the expected accuracy of these data must be assessed at different space and time scales.

Several authors have already addressed this problem. *Wyrtki* [1987], comparing maps of Geosat sea surface topography with tide-gage records at six islands in the equatorial Pacific, concludes that the sea level low-frequency behavior is well reflected on time scales greater than 2 weeks, and intuits a good comparison on space scales greater than a thousand kilometers. *Cheney et al* [1989] address the pertinent question of Geosat data quality through analysis of altimeter observations. They performed comparisons of Geosat data, both from the Geodetic Mission and the ERM, with in situ measurements (14 tide-gages, two equatorial moorings) and wind-driven model results throughout the Pacific. They demonstrate that altimetric time series have a rms accuracy of about 4 cm. *Tai et al.* [1989] find good agreement between XBT-derived dynamic heights (0/400 dbar), island sea level observations, and crossover differences from the Geodetic Mission.

In the western tropical Pacific, several independent data sets are available to compute dynamic height anomalies that allow further validation of GSLA. During the November 1986 to November 1987 period, several cruises were carried out in the vicinity of the 165°E meridian: three from the SURTROPAC (Surveillance Trans-Océanique du Pacifique) (labeled 2 and 5 on Figure 3) and PROPPAC (Production Pélagique dans le Pacifique) (labeled 6 on Figure 3) programs, two from the US-PRC (United States-People's Republic of China) bilateral cooperative program (labeled 1 and 7 on Figure 3), and the JENEX 01 (Japanese El Niño Experiment 01) (labeled 3 on Figure 3) and SAGA 2 (Study of Atmospheric Gases and Aerosols) (labeled 4 on Figure 3) cruises. Temperature data are also available from ATLAS thermistor chain moorings

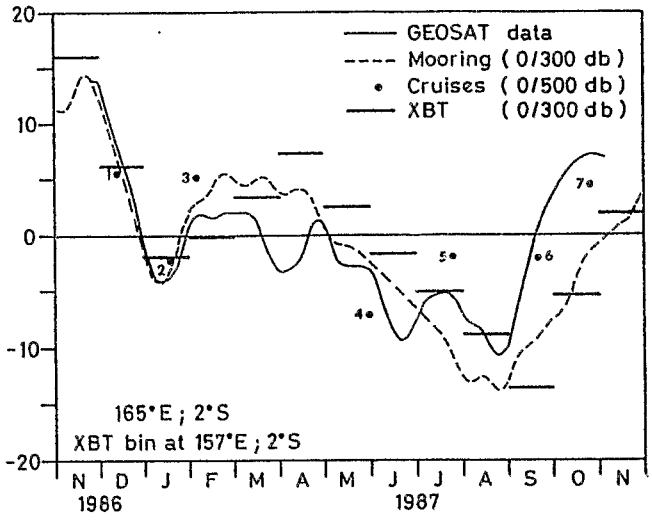

Fig. 3. Comparison between Geosat sea level anomaly time series at 2°S-165°E (solid curve), 0/300 dbar dynamic height anomaly time series obtained from an ATLAS thermistor chain mooring at 2°S-165°E (dashed curve), 0/500 dbar dynamic height anomalies derived from CTD stations during seven cruises (dots), and monthly mean 0/300 dbar dynamic height anomalies derived from XBT temperature measurements at 2°S-157°E (horizontal bars).

maintained by ORSTOM and PMEL-NOAA (Pacific Marinc Environmental Laboratory-NOAA) along 165°E, and from the TOGA ship-of-opportunity XBT network.

To compare with GSLA, 0/500 dbar dynamic heights are computed from cruise conductivity-temperature-depth (CTD) data for each station, and linearly interpolated at the closest half-degrees of latitude. The seven-cruise average height is substracted at each half-degree of latitude to provide dynamic height anomalies (DHAs). To reduce short-scale variability and filter the data similarly to GSLA data, a meridional 3° Hanning filter is also applied to these DHAs. A linear regression fit of GSLAs and DHAs at each half-degree of latitude from 20°S to 10°N is computed for all seven cruises, leading to a rms scatter of 3.8 cm about the fitted line, and a correlation coefficient of 0.71. More information on these results can be found in the work by *Eldin and Delcroix* [1989].

Temperature data from XBTs obtained along the Nouméa-Japan shipping route in the 20°S-20°N band are monthly averaged in bins of 2° of latitude by 10°-15° of longitude. Surface dynamic heights (0/300 dbar) are then computed using annual mean T-S relations [*Levitus*, 1982], and DHAs are obtained by removing the mean dynamic height from each bin. Linear regression analysis of GSLAs versus XBT DHAs, in each bin and for each month of the ERM period, leads to a rms scatter of 3.7 cm, with a correlation coefficient of 0.54.

Finally, a time series of dynamic height is also computed from the ATLAS mooring at 2°S-165°E, which provides the most complete record of the ATLAS network along 165°E. After linear interpolation across a data gap from May 20 to July 21, 1987, 0/300-dbar DHAs are obtained from daily mean temperature values and an annual T-S relation. The average for the period under study is removed and a 31-day Hanning filter is applied to these DHAs, as was done for GSLA. Once again, a regression fit is performed, between GSLAs and ATLAS DHAs at 2°S, for each 5-day bin in the ERM period. The regression parameters are a rms scatter of 3.0 cm, and a correlation coefficient of 0.80.

The three regression studies cited above lead to apparently different correlation levels, depending on the type of DHAs used. Also, the number of degrees of freedom in each case cannot be precisely indicated, because of the several filtering stages applied to the data. To solve these problems, a normalization of correlation coefficients can be performed, following *Sciremammano* [1979]. When divided by the "large-lag standard error", which takes into account autocorrelations of each series, the three normalized coefficients range from 2.8 to 3.0. This indicates that GSLAs are actually correlated at the same level with each of the three DHAs sets, at a significance level greater than 99%. Differences in raw correlations originate from the various space and time scales and record lengths involved in each set.

To illustrate these comparisons, GSLA, cruise and mooring DHAs at 2°S-165°E, and XBT DHA from the bin centered at 2°S-157°E (the closest to 165°E) are presented in Figure 3. Agreement between the four time series is qualitatively good, and the time evolution is usually well described (deviations below or close to rms scatters), as is the big sea level drop in December 1986 to January 1987, and the general trend to negative anomalies in May-August 1987. Important differences occur in April 1987, where GSLA and DHA have opposite signs, and in September-October 1987, where the sea level rise is steeper in GSLA and cruise DHA than in the mooring and XBT DHAs. Several causes can be invoked to explain these discrepancies, the first one being the different nature of measurements and processing: GSLAs are filtered in time and space, while cruise DHAs are point measurements, possibly aliased by high-frequency variability; mooring DHAs are filtered in time, but may be aliased by short spatial scale features; and XBT DHAs are averages of irregularly distributed drops. Another source of errors is the use of extraneous data to compute GSLA and DHA. Tropospheric water content corrections applied to altimeter data are derived from operational models or climatology, and they may not be entirely valid in a period of strong modifications of atmospheric variables, like the 1986-1987 ENSO [*Zimbelman and Busalacchi*, 1990]. For similar reasons, the use of a mean T-S relation in the computation of DHA leads to wide differences between in situ cruise DHA and mooring and XBT DHAs computed from mean T-S relations in the second half of 1987 [*Hénin*, 1989].

Geostrophic current anomalies. Owing to the ratio $1/f$ in (1) and to the weakness of the β term in (2), geostrophic currents are very sensitive to sea level noise close to or at the equator. From the preceding sections, we estimate that our GSLA have an error of about 4 cm, uncorrelated over 3° latitude. For such a decorrelation length, the finite derivative calculation on (1) and (2) corresponds to a maximum error in the zonal geostrophic current of 61 cm s^{-1} at the equator, 19 cm s^{-1} at 5° latitude, and 9 cm s^{-1} at 10° latitude. These theoretical errors have, in fact, the same magnitude as the surface currents in the equatorial Pacific, which are known to be stronger on than off the equator [e.g., *Wyrtki and Kilonsky*, 1984; *Delcroix et al.*, 1987].

Picaut et al. [1990] compared measured equatorial zonal current at three moorings at 165°E, 140°W, and 110°W, with zonal surface geostrophic current deduced from the second derivative equation (equation (2)) applied to the present GSLA data. The consistency between low-frequency observed currents and calculated currents was remarkably good (correlation coefficient over 0.8 and rms difference about 20 cm s^{-1}), except at the 110°W site, where most of the Geosat descending tracks are incomplete. Figure 11, adapted from *Picaut et al.* [1990], illustrates the comparison at 0°, 165°E. Although we used a slightly different technique than Picaut et al. in processing the original Geosat data, our Geosat-derived currents are essentially the same as the ones they obtained. For example, the rms difference between our calculated current and the low-pass filtered observed current at 165°E is only 25 cm s^{-1}. It must be pointed out that such rms is 2-3 times smaller than our error estimate for the current on the equator. This difference may be due to an underestimate of the 3° meridional decorrelation scale, and/or to the systematic addition of sea level errors, both used in the finite difference estimation of geostrophic current error. Off the equator, one must similarly expect a smaller error in geostrophic current than the one previously estimated. However, in the equatorial wave guide, a meridional pressure gradient can destroy the geostrophic balance; at higher latitudes, the Ekman drift might have to be added to the geostrophic current in order to get a realistic surface current [*Arnault*, 1987]. Unfortunately, a direct observation of current is not available off the equator during our period of GSLA measurements, and a precise evaluation of off-equatorial zonal geostrophic surface current cannot be made.

Keeping all of these restrictions in mind, it is, however, noteworthy that our analysis of different "sea level" data sets leads to comparable rms differences of the order of 4 cm, which confirms previous studies. In addition, surface geostrophic zonal current anomalies derived from Geosat appear to be reasonable, even on the equator, where one can expect the largest inaccuracies. Hence large-scale and low-frequency sea level and surface current are expected to show up with the present processed Geosat data.

3. SEA LEVEL VARIATIONS

As mentioned in section 1, sea level variations observed in the western equatorial Pacific will be explained in terms of linear theory of equatorial waves. A brief outline is first presented to establish the framework of our data analysis.

In nondimensional form, the dispersion relation of the equatorially trapped waves is given by

$$\omega^2 - k\omega^{-1} - k^2 = 2m + 1 \qquad (4)$$

where m is the meridional mode number. The nondimensional frequency ω and wave number k are scaled from their dimensional counterparts by the usual equatorial scaling, $T = (\beta c_n)^{-1/2}$ for the time scale, and $L = (\beta^{-1} c_n)^{1/2}$ for the length scale, where c_n is the phase speed of the nth baroclinic mode equatorially trapped Kelvin wave. Solutions for surface elevation (η) and velocity (u) are expressed in terms of the Hermite functions

$$\Psi_m(y) = \pi^{-1/4} (2^m m!)^{-1/2} \exp(-y^2/2) H_m(y) \qquad (5)$$

where H_m is the mth Hermite polynomial.

For the Kelvin waves, the surface elevation η and zonal velocity u fields are

$$\eta = u = \Psi_0(y) \exp(ikx - \omega t) \qquad (6)$$

For the long low-frequency Rossby waves ($m \geq 1$), they become

$$\eta = 2^{-3/2} [(m+1)^{-1/2} \Psi_{m+1}(y) + m^{-1/2} \Psi_{m-1}(y)] \exp(ikx - \omega t) \qquad (7)$$

$$u = 2^{-3/2} [(m+1)^{-1/2} \Psi_{m+1}(y) - m^{-1/2} \Psi_{m-1}(y)] \exp(ikx - \omega t) \qquad (8)$$

A representation of the meridional structures of these waves is given by *Eriksen* [1982; Figure 3]. For our contention, one should note that (1) at low frequency, Kelvin waves as well as long Rossby waves are nondispersive and have η and u in

geostrophic balance, and (2) the phase (= group) speeds of the equatorial Kelvin wave c_k and Rossby wave c_r are related through the following relationship

$$c_r = c_k / (2m+1), \quad (9)$$

Figure 4 shows the GSLAs along the 165°E longitude as a function of time and latitude. The time period, limited now to November 25, 1986, to November 5, 1987, is shorter than the period of the original data set owing to the smoothing/gridding procedure. The latitudes range from 20°S to 20°N for coherence with the next section, but only GSLA patches located in the equatorial band and whose amplitudes exceed 6-8 cm will be further sequentially analyzed. In support of this analysis, Figure 5 shows the 1°S-1°N average wind stress anomaly (reference November 1986 to November 1987) obtained from the Florida State University (FSU) on a monthly basis and on a 2° square grid. A constant drag coefficient $C_d = 1.2 \times 10^{-3}$ is used to convert to stress unit.

In the equatorial wave guide, the first notable GSLA patch (Figure 4) occurs in November-December 1986, with an amplitude of > 12 cm. The occurrence of the maximum is not well defined on the GSLA time series, but complementary studies dealing with longer time series of crossover Geosat sea level, island sea level, and dynamic height suggest that the maximum elevation is in mid-November 1986 [*Miller et al.*, 1988; *McPhaden et al.*, 1990]. The GSLA rise is consistent with the equatorial downwelling induced by a westerly wind anomaly located west of 170°W (Figure 5). *Miller et al.* [1988] concluded that wind variations induce a downwelling equatorial Kelvin wave that propagates at a 2.4 m s^{-1} mean phase speed between 170°E and 98°W. With the present GSLA data set, Figure 6 demonstrates such an equatorial eastward propagation from the dateline to the eastern Pacific coast. A mean phase speed $c_k = 2.26 \pm 1.04$ m s^{-1} (the second number is one standard deviation) was estimated by a time-lag correlation matrix analysis performed for the November 1986 to January 1987 period, every 10° longitude and east of the dateline in order to avoid most of the expected local wind forcing. This phase speed estimate suggests that an equatorial Kelvin wave solution (see equation (6)) may best fit the meridional (y) structures of the GSLA, i.e., the ones corresponding to the downwelling Kelvin wave. Using the least squares technique, we fit the positive GSLA meridional structures to the function

$$\eta(y) = \eta_0 \exp(-\beta y^2 / 2c) \quad (10)$$

at the dates of maximum equatorial GSLA associated with the passage of the wave, every 10° zonal grid and east of the dateline (cf. Table 1). Allowing both η_0 and c to vary, the best fits, presented in Figure 7 at different longitudes, yield well-defined and unique (η_0, c) couples, with a mean phase speed of $c_k = 2.82 \pm 0.96$ m s^{-1}. Both phase speed estimates (c_k and c_k) are in good agreement with the results of the linear theory based on observed Brunt-Väisälä frequency profiles and vertical mode decomposition. Specific estimations for the first baroclinic mode (n=1) phase speed range from 2.91 m s^{-1} near the dateline [*Eriksen*, 1982], 2.46 m s^{-1} near 150°W [*Rothstein*, 1984], to 2.10 m s^{-1} near 110°W [*Hayes and Halpern*,1984]. From *Levitus*' [1982] climatological data, the n=1 equatorial Kelvin wave phase speed ranges from 2.60 to 1.90 m s^{-1} between the dateline and the eastern coast, with a 2.25 m s^{-1} mean zonal value [*Sombardier*, 1989]. Our phase speed estimates, together with the shape of the GSLA meridional structure, thus convincingly suggest that the November-December 1986 downwelling equatorial Kelvin

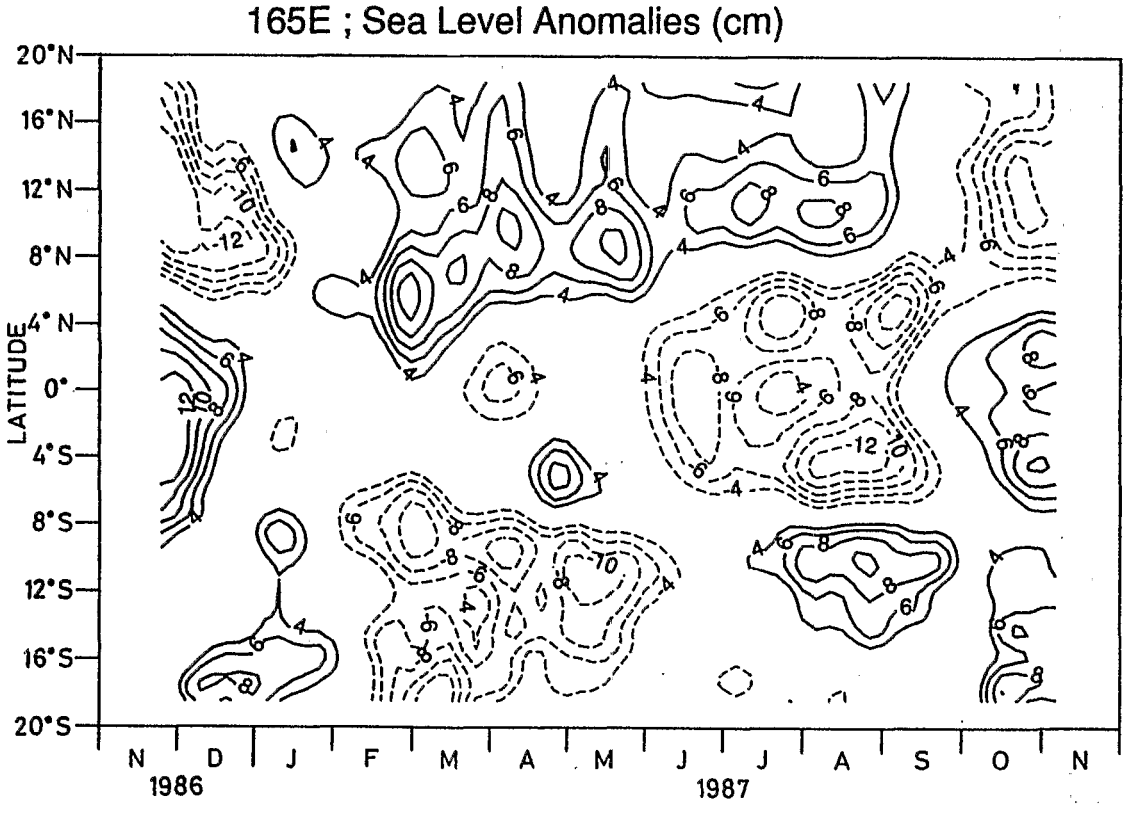

Fig. 4. Geosat sea level anomalies as a function of time and latitude, along the 165°E longitude. Contour intervals are 2 cm. The 0 and 2-cm contours are dropped for clarity.

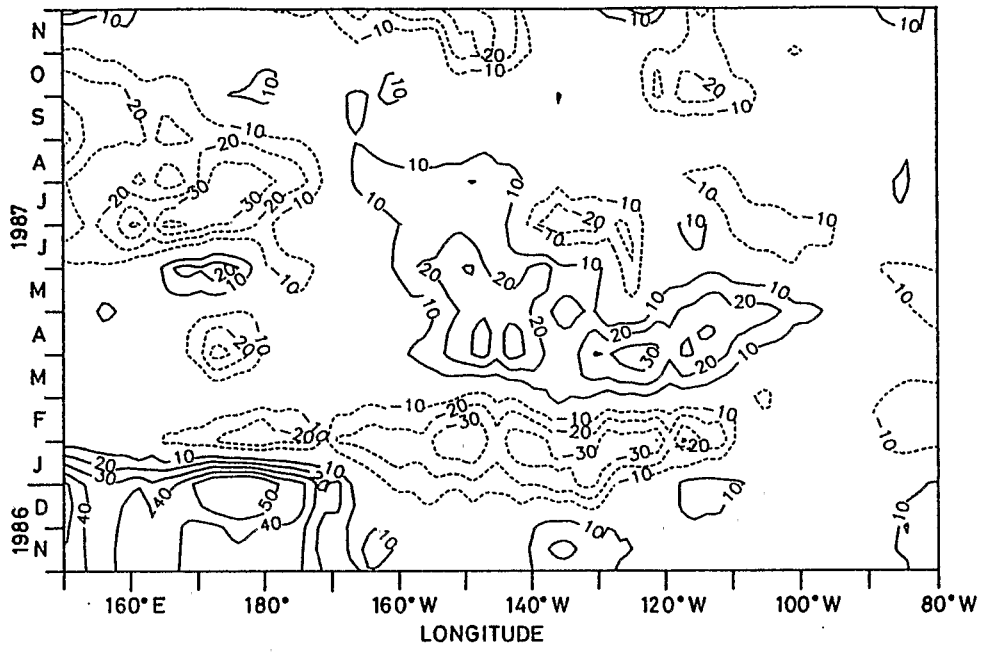

Fig. 5. Zonal wind stress anomalies along the equator as a function of time and longitude. Contour intervals are 10^3 N m^{-2}. The 0 contour is dropped for clarity.

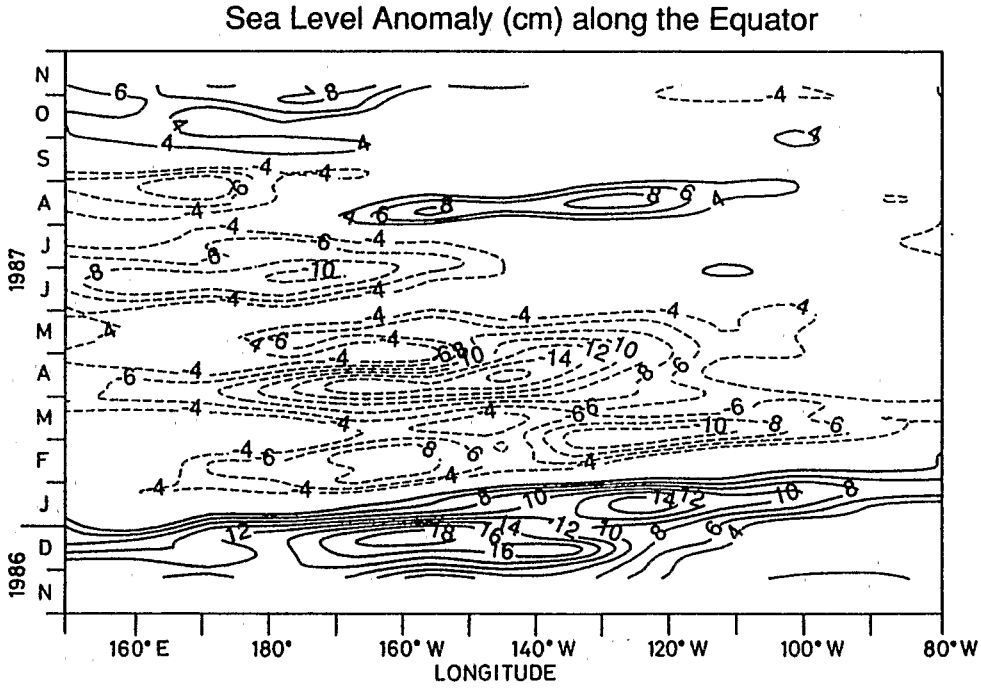

Fig. 6. Geosat sea level anomalies along the equator, as a function of time and longitude. Contour intervals are 2 cm. The 0 and 2-cm contours are dropped for clarity.

wave has the characteristics of a first baroclinic mode (n=1).

The second notable GSLA patch (Figure 4) occurs in March-April 1987. At that time, the less than -6 cm equatorial GSLA decrease could be related to the easterly wind stress anomaly centered near 170°E. Despite its relative weakness and short duration in comparison with the preceding anomaly, this patch is worth reporting because it corresponds to a -50 cm s^{-1} zonal surface geostrophic current anomaly to be detailed in section 4.

The third notable equatorial GSLA patch (Figure 4) starts in early June 1987, reaches an extremum of less than -8 cm and stops at the beginning of July 1987. Figure 5 suggests that it is

TABLE 1. Dates of Peak Sea Level at Various Longitudes Along the Equator Associated With the Downwelling Equatorial Kelvin Wave, as Shown in Figure 6

Longitude, °W	Date	Phase speed, m s^{-1}
175	Dec. 21, 1986	1.55
165	Dec. 21, 1986	3.00
155	Dec. 26, 1986	3.77
145	Dec. 21, 1986	3.96
135	Jan. 10, 1986	2.24
125	Jan. 15, 1987	3.74
115	Jan. 15, 1987	3.40
105	Jan. 25, 1987	2.09
95	Jan. 25, 1987	1.62

The third column gives the phase speed estimated from least squares fits of the positive Geosat sea level meridional structures to theoretical downwelling Kelvin wave shape, as plotted in Figure 7. Mean and standard deviation are 2.82 ± 0.96 m s^{-1}.

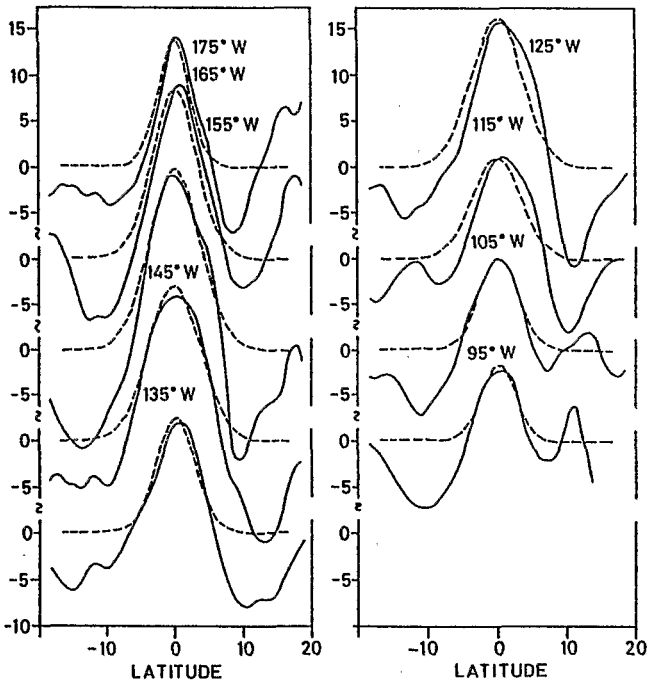

Fig. 7. Least squares fits of the positive downwelling Geosat sea level anomalies (in centimeters; solid curves) to the theoretical meridional structures (dashed curves) of an equatorial downwelling Kelvin wave (cf. equation (10)), at different longitudes (175°-95°W), and at the times reported in Table 1.

most likely related to the change in the wind-stress anomaly, from westerly to easterly, which occurs in early June 1987 near 170°E [see *McPhaden et al.*, 1990]. This wind-stress change apparently induces an upwelling equatorial Kelvin wave (Figure 6) which propagates eastward to about 150°W. Since the wave propagation is clear only 20°-30° east of the possible forcing area, an estimate of its phase speed through time-lag correlation matrix analysis on the 10° zonal grid would be too imprecise to be conclusive. However, the negative parts of the GSLA meridional structures sampled on the dates of extremum GSLA are consistent with the shape of a first baroclinic mode upwelling equatorial Kelvin wave traveling at the previously estimated mean phase speed $c_k = 2.26$ m s^{-1}. East of 150°W, the Kelvin wave becomes poorly defined in the GSLA data. An attenuation of the Kelvin wave east of 140°W was also reported in an analysis of island sea level and surface dynamic heights recorded along the equator in May-June 1986 [*McPhaden et al.*, 1988]. These authors concluded that local wind-forced variability probably interferes with the remotely forced signal and masks the arrival of the pulse. Indeed, Figure 5 suggests that the local equatorial wind stress which is propitious to a downwelling near 150°W, may mask the sea level signature of the Kelvin wave.

After the June 1987 equatorial patch, Figure 4 shows a less than -10 cm GSLA drop in July 1987, followed by a less than -12 cm drop in late August 1987, both at 4°N latitude. These two patches are symmetrical about an equatorial minimum to a less than -10 cm drop occurring in August 1987 at 4°S. As depicted in Figures 8*a* and 8*b*, these 4°N and 4°S extremes not only occur at 165°E longitude, but also appear all across the Pacific ocean, propagating westward from the eastern part of the basin. A mean phase speed $c_r = 1.02 \pm 0.37$ m s^{-1} was estimated through time-lag correlation matrix analysis over 165°E-125°W, at 4°N and 4°S, and from mid-April to mid-October 1987. The Pacific-wide occurrence of the 4°N and 4°S extremes (Figures 8*a* and 8*b*) together with their marked symmetry about the equator (Figure 9), clearly suggest the existence of a single first meridional mode (m=1) equatorial Rossby wave. Hence the c_r phase speed is in agreement with the previous finding regarding the first baroclinic mode, because the linear theory of waves (equation (9)) predicts that the m=1 equatorial Rossby wave propagates at $c_k/3$, i.e., between 0.75 and 0.94 m s^{-1} when using $c_k = 2.26$ m s^{-1} or $c_k = 2.82$ m s^{-1}. In addition, we fit the negative part of the GSLA meridional structures to the m=1 upwelling Rossby wave solution (see equation 7)

$$\eta(y) = \eta_0 2^{-3/2} \pi^{-1/4} (1/2 + \beta y^2/c) \exp(-\beta y^2 / 2c) \qquad (11)$$

at the mean dates of estimated 4°N and 4°S extremes, every 10° zonal grid and over 165°E-95°W (cf. Table 2). Once again, the best fits (Figure 9) were all obtained for unique (η_0, c) couples, yielding a mean phase speed of 2.59 ± 0.65 m s^{-1} (or 2.43 ± 0.36 m s^{-1} if the incomplete 155°E meridional structure is ignored). Such a phase speed is representative of a first baroclinic mode (n=1) Kelvin wave. The two independent estimates of the Rossby phase speed $(2.59 \pm 0.65)/3$ and 1.02 ± 0.37 m s^{-1} quantitatively agree within their given error limits. Assuming that the linear wave theory on an equatorial β plane is the proper physics, the GSLA meridional structure, together with the estimated phase speeds, are thus in excellent agreement with a n=1 and m=1 equatorial Rossby wave. An interesting question remaining is the origin of the n=1 and m=1 Rossby wave. This will be dealt with in section 5, after the analysis of surface current variations presented in section 4.

Figure 4 shows that the last detected near-equatorial GSLA patches occur in October-November 1987. Once again, the two GSLA uplifts greater than 8 cm, symmetrical about an equatorial minimum, suggest a n=1 and m=1 downwelling equatorial Rossby wave. This is to some extent corroborated by Figure 8, which indicates that these patches might originate from the eastern Pacific at a mean Rossby wave phase speed similar to the one previously estimated. However, the relevant GSLA data were too noisy and the signal too weak to be conclusive.

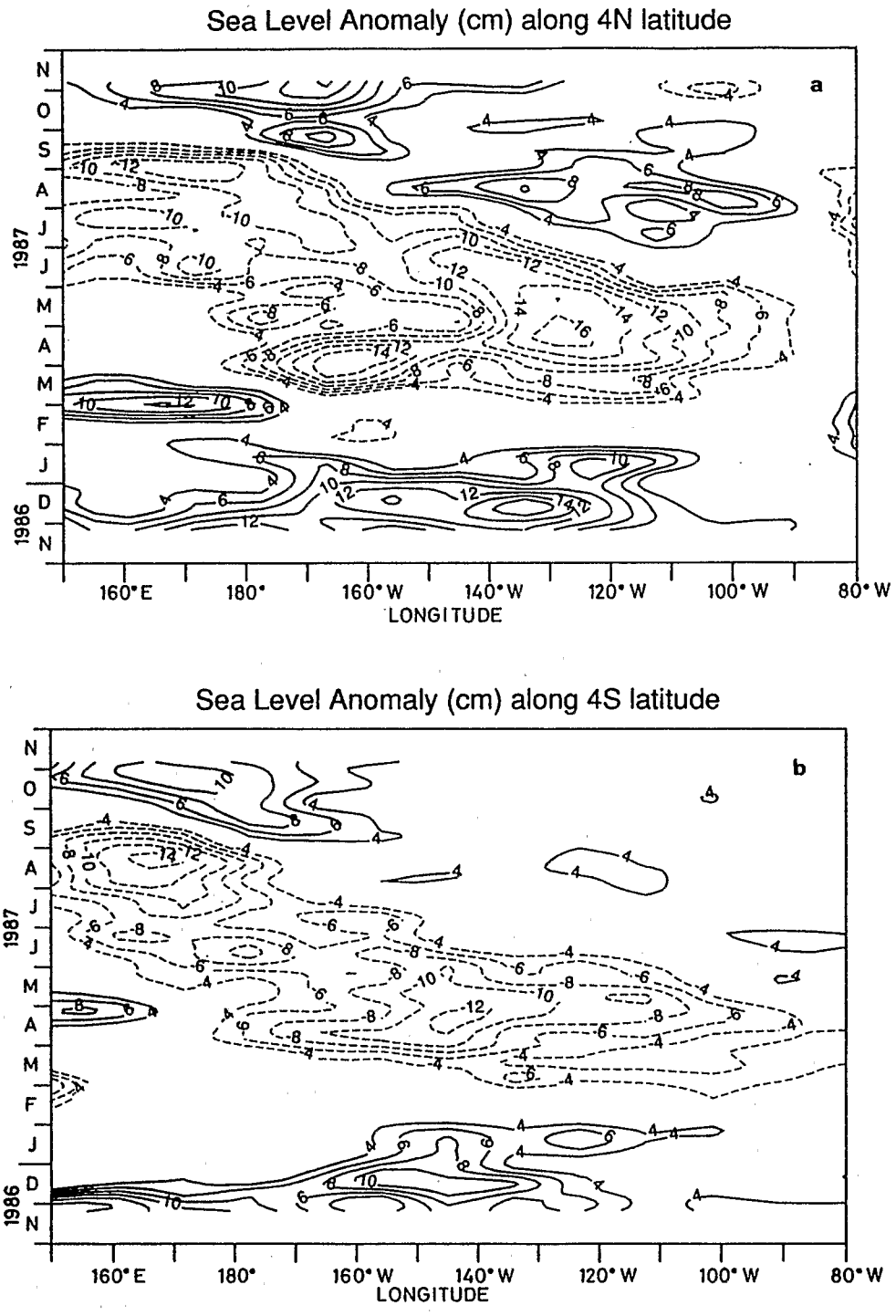

Fig. 8. Geosat sea level anomalies along (*a*) 4°N latitude and (*b*) 4°S latitude, as a function of time and longitude. Contour intervals are 2 cm. The 0 and 2-cm contours are dropped for clarity.

4. SURFACE CURRENT VARIATIONS

In the previous section we focused on the major GSLA equatorial patches along 165°E and showed that they could be interpreted as equatorial Kelvin and Rossby waves. In a similar manner, we now present the corresponding Geosat geostrophic zonal current anomalies. Despite the fact that the geostrophic anomalies are only deduced from meridional derivatives (equations (1) and (2)) of GSLA patches, the following representations and analyses can usefully complement the previous chapter. Once again, the reader must keep in mind that the GZCA are relative to their means over the November 1986 to November 1987 period. An estimate of these means at the equator has been deduced from the observed currents by *Picaut et al.* [1990]. At 165°E, 140°W, and 110°W, they are 19, -13, and -16 cm s^{-1}, respectively. Despite the El Niño condition, it appears that these relatively low means are rather close to

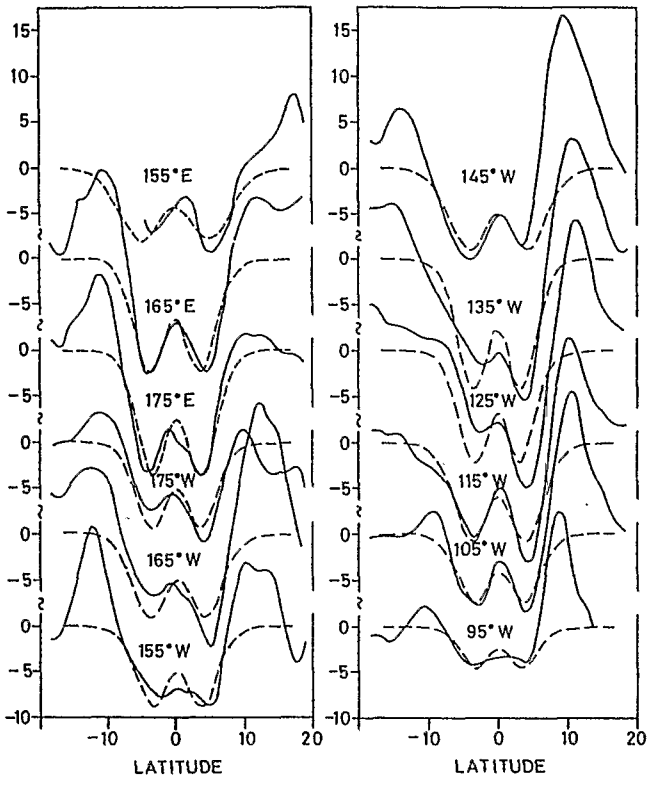

Fig. 9. Least squares fits of the negative upwelling Geosat sea level anomalies (in centimeters; solid curves) to the theoretical meridional structures (dashed curves) of an equatorial upwelling Rossby wave (cf. equation (11)), at different longitudes (155°E-95°W), and at the times reported in Table 2.

TABLE 2. Dates of Mean 4°N-4°S Peak Sea Level at Various Longitudes Associated With the Upwelling Equatorial Rossby Wave as Shown in Figures 8*a* and 8*b*

Longitude	Dates (1987)	Phase speed (m s^{-1})
155°E	Sept. 3	4.32
165°E	Aug. 29	2.44
175°E	Aug. 24	2.30
175°W	July 20	2.32
165°W	July 10	2.85
155°W	June 10	2.34
145°W	May 21	3.23
135°W	May 16	2.25
125°W	May 11	2.02
115°W	May 6	2.72
105°W	April 25	2.27
95°W	March 31	2.00

The third column gives the phase speed estimated from least squares fits of the negative Geosat sea level meridional structures to theoretical upwelling Rossby wave shape, as plotted in Figure 9. Mean and standard deviation are 2.59 ± 0.65 m s^{-1}.

normal, except at 165°E, where they are more eastward [*Delcroix et al.*, 1987; *McPhaden and Taft*, 1988].

Figure 10 represents GZCA, along the 165°E longitude, as a function of time and latitude. As expected, it shows that the strongest surface current variations are located in the equatorial wave guide, the standard deviations of the currents being 44, 17, 5, and 3 cm s^{-1} at 0°, 5°N, 10°N, and 15°N, respectively. In turn, such a meridional distribution raises doubt about the significance of our calculated currents, owing to its similarity to the theoretical errors we described in the calculation technique. As shown in Figure 11 and detailed in section 2.3, direct comparisons between Geosat-derived and measured currents give a mean rms difference of 25 cm s^{-1} at the equator, a value which is half the theoretical error and, more importantly, 2-3 times smaller than the signals we analyzed. Off the equator, there is no way to get a precise estimate of GZCA error, but it is very probably smaller than the uncertainty on the equator. We therefore believe that the main GZCA signals depicted on Figure 10 are significant.

With the ratio $1/f$ in (1), the equatorial trapping of the GZCA Kelvin waves turns out to be more apparent in Figure 10 than with the sea level anomalies in Figure 4. The downwelling Kelvin wave, generated in November-December 1986, has a surface eastward current signature with a maximum of 50 cm s^{-1} right at the equator. The second aforementioned GSLA patch in March-April 1987 shows up in GZCA as a westward surface flow anomaly as large as -50 cm s^{-1}. There is no strong current associated with the upwelling equatorial Kelvin wave evidenced in GSLA in June-July 1987. The combination of local wind forcing (cf. Figure 5) and/or incoming equatorial Rossby wave (Figure 9), which, as seen below, has a current signature maximum at the equator, might blur this last phenomenon.

Contrary to the case of an equatorial Kelvin wave, the theoretical shape of zonal currents associated with an equatorial Rossby wave (Figure 12) is very different from its sea level representation (Figure 8). It appears as a strong, equatorially trapped current flanked on the northern and southern sides by two opposite currents of smaller amplitude. In Figure 10, and along 165°E, such a current structure shows up in July-September 1987 from the aforementioned GSLA equatorial Rossby wave. At the equator there flows an eastward anomaly of up to 60 cm s^{-1}, surrounded by two westward current anomalies down to -20 cm s^{-1}. This equatorial Rossby wave current structure is more evident in the central and eastern Pacific. For example, at 145°W (Figure 12), a least squares fit of the meridional current structure to the function

$$U(y) = U_0\, 2^{-3/2}\, \pi^{1/4}\, (-3/2 + \beta y^2/c) \exp(-\beta y^2 / 2c) \quad (12)$$

corresponds to a phase speed of 2.75 m s^{-1}, in agreement with our previous results. The equatorial Rossby wave GZCA propagates westward but, in contrast with the GSLA structure, it is not clearly defined over the whole tropical Pacific basin. Figure 13 illustrates the time/space sequence when the Rossby wave is the most evident in the surface current structure. The equatorially trapped current anomaly (50 to 80 cm s^{-1} maxima), accompanied by the northern and southern westward current anomalies (-20 to -40 cm s^{-1} maxima), propagate between April 15 to June 1 from the eastern to the central tropical Pacific at a mean phase speed of about 0.75 m s^{-1}. This propagating current structure disappears and reappears near 165°E in July-August (Figure 10). Between 150°W and the dateline, the equatorial Rossby wave GZCA may be masked by other equatorial phenomena (Figure 6) or imprecise Geosat data between 150°W and the dateline (Figure 1).

Two conclusions can be drawn from the last sections. First, the GZCA structure associated with the equatorial Rossby wave not only influences the currents within the equatorial wave guide (as with Kelvin waves), but also affects most of the

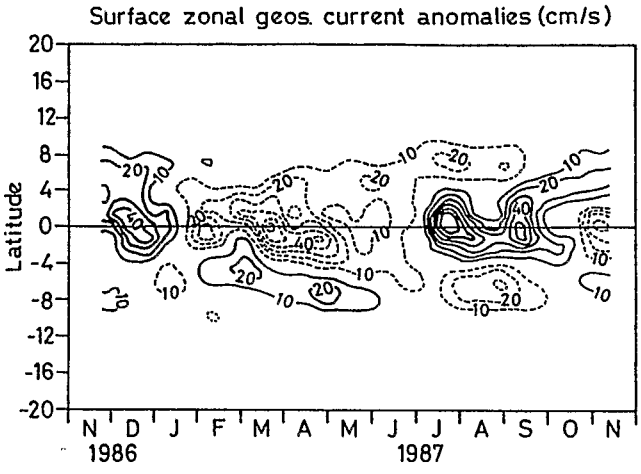

Fig. 10. Zonal surface geostrophic current anomalies as a function of time and latitude, along the 165°E longitude. Contour intervals are 10 cm s^{-1}. The 0 contour is dropped for clarity.

surface equatorial currents. Figure 13 clearly indicates that the North Equatorial Countercurrent (NECC) and South Equatorial Countercurrent (SECC) are strongly affected by the passage of the first vertical, first meridional mode equatorial Rossby wave. Second, and unlike the GSLA Rossby wave structure which is obvious only west of 100°W (Figure 9), it seems that the corresponding GZCA structure emanates from the South American coast (cf. first panel of Figure 13).

5. Conclusion and Discussion

In this paper, specific additional processing of the corrected Geosat sea level data enables us to demonstrate that the major large-scale low-frequency changes of sea level and zonal geostrophic surface current anomalies can be explained by the linear theory of equatorial waves. In particular, the downwelling equatorial Kelvin wave generated in the western Pacific in December 1986 is carefully analyzed, since it is the dominant oceanic signal of the 1986-1987 El Niño. A time-lag correlation matrix analysis and an estimate of the equatorial trapping scale independently indicate that this equatorial wave has the characteristic of a first baroclinic mode. Moreover, our study provides, for the first time, comprehensive evidence of a first meridional first baroclinic equatorial Rossby wave whose sea level and surface current anomaly signatures clearly propagate over most of the equatorial Pacific basin.

The equatorial waves were unambiguously identified by their phase propagation and meridional structures. It is now opportune to discuss and suggest tentative explanations for the generation of the waves.

With regard to the equatorial Kelvin waves, we systematically noticed the good time agreement between their appearance and the existence of notable zonal wind stress anomalies. In other words, we suggested that the wind change might be the local generating mechanism. Our argument is based on analysis of limited available data, and is thus subject to a minimum of caution. First, detailed examination of Figures 5 and 6 reveals specific wind events that do not result in observable waves. Second, an equatorial Kelvin wave could also be generated remotely in response to the incidence of an off-equatorial Rossby wave upon the coast of Asia [*White et al.*, 1985, 1987; *Pazan et al.*, 1986]. The limited 1-year period of available Geosat data, the poor density of the data for the far western Pacific, and the fact that wind stress values are only available on a monthly basis clearly prevent us from being categorical about the connection between wind stress anomaly and generation of Kelvin waves.

The mechanism responsible for the upwelling equatorial Rossby wave also remains to be elucidated. The following

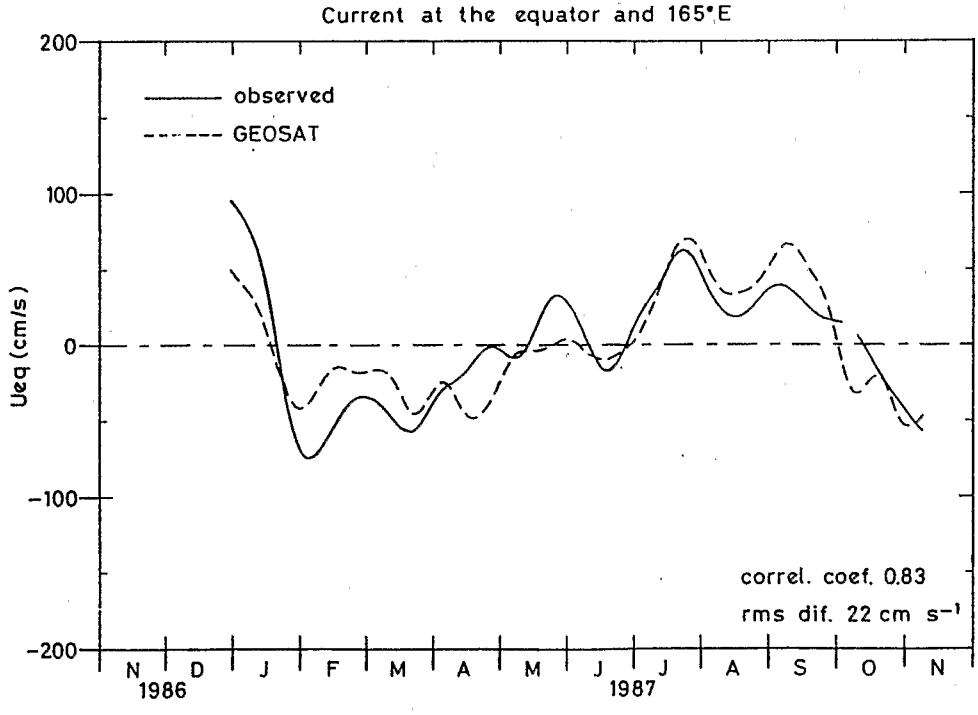

Fig. 11. Zonal surface geostrophic current estimated from Geosat (dashed curve), and near-surface zonal current measured directly from an equatorial mooring at 165°E longitude (solid curve) [from *Picaut et al.*, 1990].

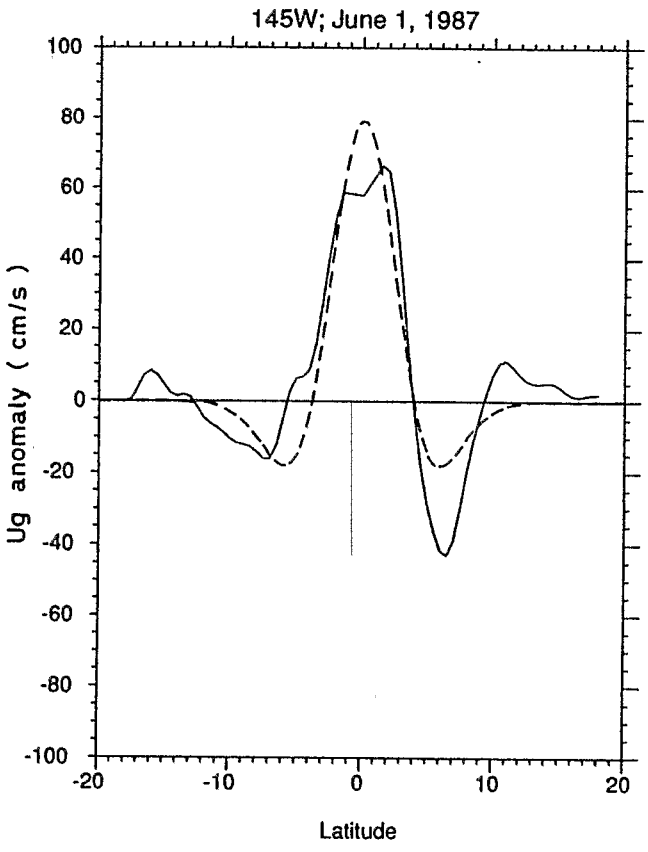

Fig. 12. Least squares fit of the Geosat-derived zonal surface geostrophic current anomalies (in cm s^{-1}; solid curve) to the theoretical meridional structure (dashed curve) of an equatorial upwelling Rossby wave (cf. equation (12)), at 145°W longitude and on June 1, 1987.

paragraph presents information suggesting that the Rossby wave is most probably caused by the reflection of an upwelling equatorial Kelvin wave at the eastern Pacific boundary.

Figure 6 shows an upwelling equatorial Kelvin wave (8- to 10-cm sea level drop) crossing the entire Pacific basin from near the dateline in January-February 1987 to the eastern coast by the end of March 1987. Once again, the origin of this Kelvin wave is consistent with the occurrence of an easterly wind stress anomaly patch. Time-lag correlation matrix analysis, together with the meridional trapping scale study, confirm that this wave has the characteristics of a first baroclinic mode. Owing to the good agreement in time at the eastern boundary, Figures 6, 8*a*, and 8*b* suggest that the equatorial upwelling Kelvin wave could reflect as an equatorial upwelling Rossby wave, though the weakness of the associated sea level structures at the eastern boundary prohibits any firm conclusion. However, starting from the end of March 1987 and using the 0.94 m s^{-1} mean phase speed of the Rossby wave (cf. section 3), a reflected Rossby wave would cross the 165°E meridian around September 1, 1987, i.e., in good agreement with what is depicted in Figure 4. Furthermore, Figure 13 does show a strong surface current Rossby wave signature at the eastern coast, simultaneously with the arrival of the Kelvin wave. Therefore the equatorial upwelling Rossby wave appears to be the result of the reflection of the equatorial upwelling Kelvin wave. In this context, it is surprising to notice that the December 1986 equatorial downwelling Kelvin wave (Figure 6) does not induce a reflected Rossby wave (Figure 8). A first baroclinic linear model was

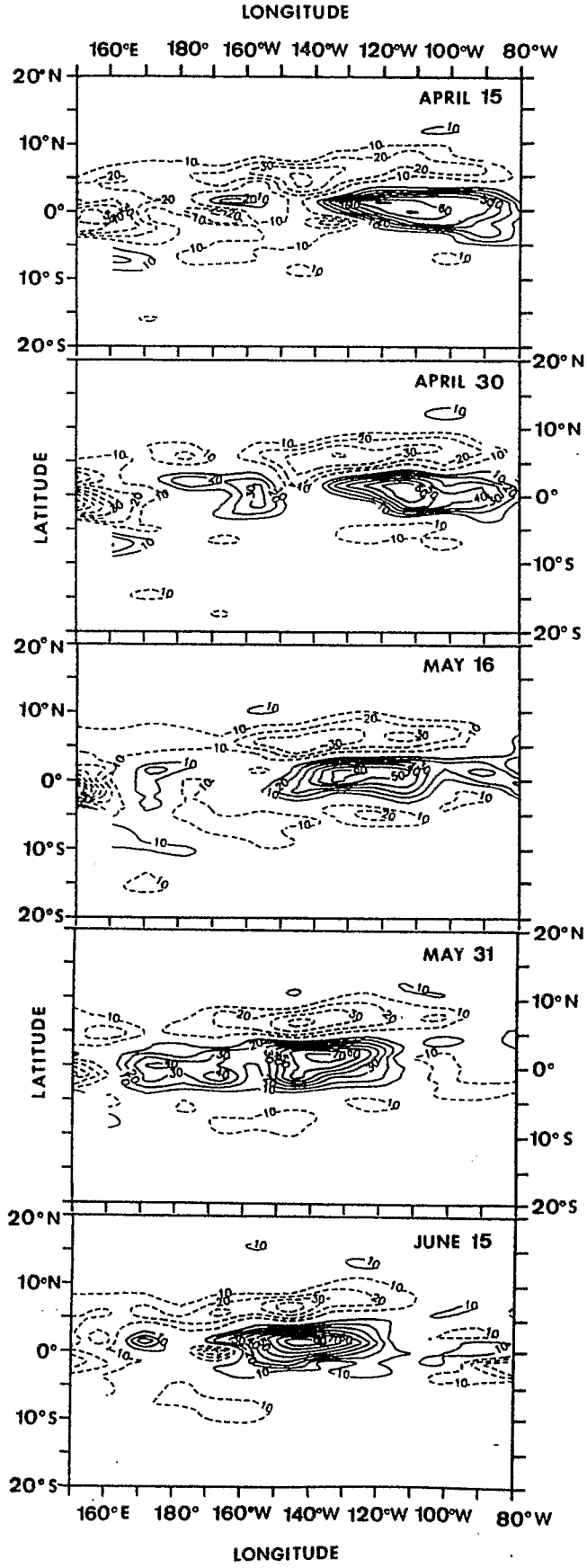

Fig. 13. Time/space representation of the Geosat zonal surface geostrophic current anomalies from April 15 to June 15, 1987. Contour intervals are 10 cm s^{-1}. The 0 contour is dropped for clarity. It depicts the westward propagation of the upwelling equatorial Rossby wave from the eastern to the central Pacific.

thus used to assess the feasibility of the downwelling and upwelling Rossby wave reflections (Y. duPenhoat, personal communication, 1989).

On one hand, when the model is forced with the FSU wind stress anomaly, the downwelling (December 1986) and upwelling (January-February 1987) equatorial Kelvin waves are obvious. A downwelling Rossby wave does not show up, in contrast with an upwelling Rossby wave that clearly reflects at the eastern Pacific coast. The propagations of these simulated equatorial waves are thus in excellent agreement with the ones deduced from the Geosat sea level data.

On the other hand, when the model is forced with the same wind stress anomaly but excluding the contribution of the locally forced Rossby wave, the downwelling and upwelling Kelvin waves still appear but with a different future after they reach the eastern Pacific coast. Indeed, a downwelling Rossby wave shows up, whereas the upwelling Rossby wave is still present but reduced in sea level amplitude. These features suggest that in the eastern part of the basin the local response of the wind does weaken the reflected downwelling Rossby wave, but it enhances the reflected upwelling Rossby wave. As far as the model output can be trusted, the contribution of the local wind is responsible for the absence of a reflected downwelling Rossby wave.

Another question raised by our study is whether the detected equatorial Kelvin and Rossby waves belong to the 1986-1987 El Niño or are parts of the "normal" seasonal cycle. This distinction is essential, since we showed that these equatorial waves strongly affect the three main surface currents (NECC, South Equatorial Current (SEC), SECC), therefore changing the redistribution of mass and heat over the equatorial basin. Once again, a linear model (Y. duPenhoat, personal communication, 1989) was used to answer this question in the absence of several years of Geosat ERM sea level time series. A mean seasonal cycle of simulated sea level was obtained from the linear model forced with the climatological FSU wind stress (mean over the 1961-1988 period). Interestingly, the structure and timing of this sea level mean seasonal cycle are similar to the main features associated with what we observed during the 1986-1987 El Niño. In other words, the 1986-1987 downwelling and upwelling equatorial Kelvin waves, together with the reflected upwelling equatorial Rossby wave, could be part of the normal seasonal cycle. In this case, the anomalous surface currents associated with these equatorial waves would be able to seasonally modify the sea surface temperature field through advective processes [cf. *Harrison and Schopf*, 1984]. Clearly, the role of the observed surface current anomalies, in creating or not creating an El Niño situation, deserves investigation.

Forthcoming improvement of altimeter sea level accuracy and increasing length of sea level time series will enable us to refine our conclusions. In this context and in view of the results already obtained with Geosat, the future TOPEX/POSEIDON mission, which will provide an unprecedented high-quality sea level coverage, is likely to contribute greatly to our understanding of the physics governing the low-frequency variability of the equatorial oceans.

Acknowledgments. This work could not have been carried out without the Geosat ERM preprocessed data kindly provided by Chet Koblinsky, and the programming support of François Masia. Discussions with Yves duPenhoat were very valuable. A set of complementary data was generously provided by Kei Muneyama (JENEX cruise), Jim O'Brien (FSU wind stress), Marie Hélène Radenac (PROPPAC cruises), Lynne Talley (SAGA cruise), and John Toole (US-PRC cruises). Marina Laplagne gave pertinent editing suggestions. Support for this work, as part of the TOPEX/POSEIDON Science Working Team, was provided by the Programme de Télédetection Spatiale, through Actions Incitatives sur Programmes 59.88.46 and 9.88.25. All these contributions are gratefully acknowledged.

REFERENCES

Arnault, S., Tropical atlantic geostrophic currents and ship drifts, *J. Geophys. Res., 92*, 5076-5088, 1987.

Battisti, D. S., On the role of off-equatorial oceanic Rossby waves during ENSO, *J. Phys. Oceanogr., 19*, 551-559, 1989.

Bendat, J., and A. Piersol, Random data analysis and measurement procedures, Wiley Interscience, New York, 407 pp., 1971.

Busalacchi, A., and J. J. O'Brien, Interannual variability of the equatorial Pacific in the 1960s, *J. Geophys. Res., 86*, 10,901-10,907, 1981.

Cane, M. A., and E. S. Sarachik, Equatorial oceanography, *Rev. Geophys., 23*, 1137-1148, 1983.

Cheney, R. E., and L. Miller, Mapping the 1986-87 El Niño with Geosat, *Eos Trans. AGU, 69*, 754-755, 1988.

Cheney, R. E., J. G. Marsh, and B. D. Beckley, Global mesoscale variability from collinear tracks of Seasat altimeter data, *J. Geophys. Res., 88*, 4343-4354, 1983.

Cheney, R. E., B. C. Douglas, R. W. Agreen, L. Miller, and D. L. Porter, Geosat altimeter geophysical data record user handbook, *NOAA Tech. Memo., NOS NGS-46*, 29 pp., Natl. Oceanic and Atmos. Admin., Rockville, Md., 1987.

Cheney, R. E., B. C. Douglas, and L. Miller, Evaluation of Geosat altimeter data with application to tropical Pacific sea-level variability, *J. Geophys. Res., 94*, 4737-4749, 1989.

Delcroix, T., G. Eldin, and C. Hénin, Upper ocean water masses and transports in the western tropical Pacific (165°E), *J. Phys. Oceanogr., 17*, 2248-2262, 1987.

Eldin, G., and T. Delcroix, Vertical thermal structure variability along 165°E during the 1986-87 ENSO event, in *Proceedings of the Western Pacific International Meeting and Workshop on TOGA-COARE*, edited by J. Picaut, R. Lukas, and T. Delcroix, Centre ORSTOM de Nouméa, New Caledonia, 269-281, 1989.

Emery, W. J., and L. Magaard, Baroclinic Rossby waves as inferred from temperature fluctuations in the eastern Pacific, *J. Mar. Res., 34*, 365-385, 1976.

Eriksen, C., Equatorial wave vertical modes observed in a western Pacific island array, *J. Phys. Oceanogr., 12*, 1206-1227, 1982.

Eriksen, C., and E. Katz, Equatorial dynamics, *Rev. Geophys., 25*, 217-226, 1987.

Hayes, S., and D. Halpern, Correlation of current and sea level in the eastern equatorial Pacific, *J. Phys. Oceanogr, 14*, 811-824, 1984.

Harrison, D. E., and P. S. Schopf, Kelvin-wave-induced anomalous advection and the onset of surface warming in El Niño events, *Mon. Weather Rev., 112*, 923-933, 1984.

Hénin, C., Thermohaline structure variability along 165°E in the western tropical Pacific ocean (January 1984 - January 1989), in *Proceedings of the Western Pacific International Meeting and Workshop on TOGA-COARE*, edited by J. Picaut, R. Lukas, and T. Delcroix, Centre ORSTOM de Nouméa, New Caledonia, 155-163, 1989.

Jerlov, N. G., Studies of the equatorial currents in the Pacific, *Tellus, 5*, 308-314, 1953.

JHAPL, Johns Hopkins Applied Physics Laboratory, The Navy Geosat mission, *Tech. Digest, 8-2*, 290 pp., Johns Hopkins Univ., Laurel, Md., 1987.

Joyce, T. M., Wind-driven cross-equatorial flow in the Pacific ocean, *J. Phys. Oceanogr., 18*, 19-24, 1988.

Kessler, W.S., Observations of long Rossby waves in the northern tropical Pacific, *J. Geophys. Res., 95*, 5183-5217, 1990.

Knox, R., and D. Anderson, Recent advances in the study of the low-latitude ocean circulation, *Prog. Oceanogr., 14*, 259-317, 1985.

Knox, R., and D. Halpern, Long range Kelvin wave propagation of transport variations in Pacific ocean equatorial currents, *J. Mar. Res., 40 (Suppl.)*, 329-339, 1982.

Levitus, S., Climatological atlas of the world ocean, *NOAA Prof. Pap., 13*, Natl. Oceanic and Atmos. Admin., Washington, D.C., 1982.

Lighthill, M. J., Dynamic response of the Indian ocean to onset of the southwest monsoon, *Philos. Trans. R. Soc. London, 265*, 45-92, 1969.

Lukas, R., and E. Firing, The annual Rossby wave in the Central Equatorial Pacific ocean, *J. Phys. Oceanogr., 15*, 55-67, 1985.

Lukas, R., S. P. Hayes, and K. Wyrtki, Equatorial sea level response during the 1982-1983 El Niño, *J. Geophys. Res., 89*, 10,425-10,430, 1984.

Matsuno, T., Quasi-geostrophic motions in the equatorial area. *J. Meteorol. Soc. Jpn., 44*, 25-42, 1966.

McCreary, J. P., Eastern tropical ocean response to changing wind system - with application to El Niño, *J. Phys. Oceanogr., 6*, 632-645, 1976.

McCreary, J. P., Modeling equatorial ocean circulation, *Ann. Rev. Fluid Mech., 17*, 359-409, 1985.

McPhaden, M., and B. Taft, Dynamics of seasonal and intraseasonal variability in the eastern equatorial Pacific, *J. Phys. Oceanogr., 18*, 1714-1732, 1988.

McPhaden, M., P. Freitag, S. Hayes, B. Taft, Z. Chen, and K. Wyrtki, The response of the equatorial Pacific ocean to a westerly wind burst in May 1986, *J. Geophys. Res., 93*, 10,589-10,603, 1988.

McPhaden, M., S. P. Hayes, L. Mangum, and J. Toole, Variability in the western equatorial Pacific ocean during the 1986-87 El Nino / Southern Oscillation event, *J. Phys. Oceanogr., 20*, 190-208, 1990.

Meyers, G., On the annual Rossby wave in the tropical north Pacific ocean, *J. Phys. Oceanogr.,9*, 663-674, 1979.

Miller, L., and R. E. Cheney, Large-scale meridional transport in the tropical Pacific Ocean during the 1986-1987 El Niño from Geosat, *J. Geophys. Res., 95*, 17,905-19,919, 1990.

Miller, L., R. E. Cheney, and B. C. Douglas, Geosat altimeter observations of Kelvin waves and the 1986-1987 El Niño, *Science, 239*, 52-54, 1988.

Moore, D. W., Planetary-gravity waves in an equatorial ocean, Ph. D. thesis, 207 pp., Harvard Univ., Cambridge, Mass., 1968.

Moore, D. W., and S. G. Philander, Modeling of the tropical oceanic circulation, in *The Sea*, vol. 6, pp. 319-361, Wiley-Interscience, New York, 1977.

Pazan, S., W. White., M. Inoue., and J. O'Brien, Off-equatorial influence upon the Pacific equatorial dynamic height variability during the 1982-1983 El Niño/Southern Oscillation, *J. Geophys. Res., 91*, 8437-8449, 1986.

Philander, S. G., Forced oceanic waves, *Rev. Geophys., 16*, 15-46, 1978.

Picaut, J., and R. Tournier, Monitoring the 1979-1985 equatorial Pacific current transports with expendable bathythermograph data, *J. Geophys. Res.*, this issue.

Picaut, J., A. J. Busalacchi, M. J. McPhaden, and B. Camusat, Validation of the geostrophic method for estimating zonal currents at the equator from Geosat altimeter data, *J. Geophys. Res., 95*, 3015-3024, 1990.

Ripa, P., and S. P. Hayes, Evidence for equatorial trapped waves at the Galapagos islands, *J. Geophys. Res., 86*, 6509-6516, 1981.

Rothstein, L., A model of the equatorial sea surface temperature field and associated circulation dynamics, *J. Phys. Oceanogr., 14*, 1875-1892, 1984.

Schwiderski, E. W., On charting global tides, *Rev. Geophys., 18*, 243-268, 1980.

Sciremammano, F., A suggestion for the presentation of correlations and their significance levels, *J. Phys. Oceanogr., 9*, 1273-1276, 1979.

Sombardier, L., Influence of density structure and bottom depth on vertical modal calculation in the tropical Pacific Ocean, Mémo. de stage, Sér. sci. de la mer, 57 pp., Centre ORSTOM de Nouméa, New Caledonia, 1989.

Stewart, R. H., and M. Lefebvre, TOPEX/POSEIDON: A contribution to the World Climate Research Program, in *Aerospace Century XXI*, vol. 64, edited by G. W. Morgenthaller, G. L. May, W. K. Tobiska, and J. N. Koster, pp. 117-128, American Astronautical Society, San Diego, Ca., 1987.

Tai, C. K., W. B. White, and S. E. Pazan, Geosat crossover analysis in the tropical Pacific, 2, Verification analysis of altimetric sea level maps with expendable bathythermograph and island sea level data, *J. Geophys. Res., 94*,897-908, 1989.

Tournier, R., Variabilité de la structure thermique et des courants à l'ouest et au centre de l'océan Pacifique tropical, thèse, 154 pp., Université Paris VI, Paris, 1989.

White, W. B., Secular variability in the baroclinic structure of the interior North Pacific from 1950-1970, *J. Mar. Res., 35*, 587-607, 1977.

White, W. B., G. Meyers, J.-R. Donguy, and S. Pazan, Short-term climatic variability in the thermal structure of the Pacific ocean during 1979-1982, *J. Phys. Oceanogr., 15*, 917-935, 1985.

White, W.B., S. Pazan, and M. Inoue, Hindcast/forecast of ENSO events based upon the redistribution of observed and model heat content in the western tropical Pacific, *J. Phys. Oceanogr., 17*, 264-280, 1987.

Wyrtki, K., Comparing Geosat altimetry and sea level, *Eos Trans. AGU, 68*, 731, 1987.

Wyrtki, K., and B. Kilonsky, Mean water and current structure during the Hawaii-to-Tahiti shuttle experiment, *J. Phys. Oceanogr.,14*, 242-254, 1984.

Zimbelman, D. F., and A. J. Busalacchi, The wet tropospheric range correction: Product intercomparisons and the simulated effect for tropical Pacific altimeter retrievals, *J. Geophys. Res., 95*, 2899-2922, 1990.

T. Delcroix, G. Eldin, and J. Picaut, Groupe SURTROPAC-ORSTOM, Institut Français de Recherche Scientifique pour le Développement en Coopération, BP A5, Nouméa, New Caledonia.

(Received December 27, 1989;
accepted July 3, 1990.)